TK-1-364　改 2

平成 30 年 4 月 26 日
日本原子力発電㈱

漂流物に係る検討について（コメント回答）

平成 30 年 4 月 6 日に実施したヒアリングにおけるコメントについて回答を以下に示す。

コメント①

・ Haehnel and Daly の式の引用及び適用について再検討すること。

コメント②

・ 電力中央研究所の実験における車両の軸剛性の同定において，付加質量が含まれていることの詳細を示すこと。

コメント③

・ FEMA の算定式における係数 1.3 の扱いについて，再検討すること。

1．コメント回答①（Haehnel and Daly の式の引用及び適用について再検討すること。）

FEMA の漂流物荷重算定式を表－1 に，電力中央研究所（2015）※1 及び高畠ら（2015）※2 おいて実験における実現象を再現する車両の有効軸剛性を同定するのに用いられた Haehnel and Daly※3 の式を表－2 に示す。

表－1　FEMA の漂流物荷重算定式の整理

出典	種類	概要及び算定式	算定式の適用性が確認された範囲（実験条件等）
FEMA（2012）	流木 コンテナ	$F_i = 1.3u_{max}\sqrt{km_d(1+c)}$ F_i：衝突力，c：付加質量係数， u_{max}：漂流物を運ぶ流体の最大流速， m_d：漂流物の質量，k：漂流物の有効軸剛性	「運動方程式に基づく衝突力方程式」 非減衰系の振動方程式に基づいており，衝突体及び被衝突体の両方とも完全弾性体で，かつ衝突時のエネルギー減衰が一切考慮されていない前提条件での算定式であることから，衝突時に塑性変形を伴う漂流物の荷重算定では，個別の漂流物に対して，実現象を再現するような軸剛性を適切に定める必要がある。 FEMA の原形式は，$F = v\sqrt{km}$（Haehnel and Daly※3）であり，表面流速（津波流速）ではなく漂流流速を用いて漂流物荷重を算定する式となっている。漂流物が地表面を転がるような場合は，衝突流速を 50%として良い可能性があるとの記載がある。

表－2　Haehnel and Daly の式の整理

出典	種類	概要及び算定式	算定式の適用性が確認された範囲（実験条件等）
Haehnel and Daly（2004）	車両	$F = v\sqrt{k(m_1 + Cm_f)}$ F：衝突力，v：漂流物の速度，k：漂流物の有効軸剛性， C：付加質量係数 m_1：漂流物の質量，m_f：漂流物により押し退けられた流体の質量 $F = v\sqrt{km}$ F：衝突力，v：漂流物の速度， m：漂流物の質量，k：漂流物の有効軸剛性	FEMA の原形式であり，表面流速（津波流速）ではなく漂流流速を用いて漂流物荷重を算定する式である。 原論文では，付加質量係数 C を含めた式として$F = v\sqrt{k(m_1 + Cm_f)}$が記載されているが，漂流物により除かれる流体の質量 m_f の算定は難しく，FEMA（2012）ではこれを漂流物の質量とした形で算定式が示されている。原論文には，付加質量係数 C の影響を無視した式として$F = v\sqrt{km}$が記載されている。 $F = v\sqrt{km}$は，電力中央研究所（2015）※1 及び高畠ら（2015）※2 おいて実験における実現象を再現する車両の有効軸剛性を同定するのに用いられている式である。高畠ら（2015）※2 の車両の軸剛性の同定では，衝突荷重を測定し，漂流物の質量 m は車両の質量で一定とした上で，その荷重を$F = v\sqrt{km}$で再現するように軸剛性 k を求めている。

以降に，Haehnel and Daly（2004）※3 における記載を示す。

Maximum Impact Force of Woody Debris on Floodplain Structures

Robert B. Haehnel[1] and Steven F. Daly, P.E., M.ASCE[2]

Abstract: We collided woody debris (i.e., logs) with structures using flume and test basin laboratory facilities to investigate the maximum impact force that floodplain structures are exposed to from floating woody debris. The tests also investigated the influence of collision geometry, determined by the debris orientation on impact, on the maximum impact forces. We reviewed the three approaches that represent the existing guidance for estimating maximum impact forces. Each approach estimates the maximum impact force based on the debris velocity and mass. We show that all the existing approaches can be derived from a single-degree-of-freedom model of the collision and can be considered to be equivalent. The laboratory data show that the maximum impact force was associated with a log striking a rigid structure with its end. Oblique and eccentric collisions reduced the maximum impact load in a predictable and consistent manner. The approach we refer to as "contact stiffness," a linear, one-degree-of-freedom model with no damping, was able to reproduce the laboratory results over the entire range of data, with an effective contact stiffness of 2.4 MN/m.

DOI: 10.1061/(ASCE)0733-9429(2004)130:2(112)

CE Database subject headings: Impact forces; Debris; Flood plains; Floating bodies; Flood damage.

Introduction

Debris transported by floodwaters can strike residential, commercial, or other structures in the floodplain. These impacts reduce or redirect the velocity of the debris and impart a force to the structure. The magnitude of the force can be large enough to cause substantial, or even catastrophic, damage to the structures. Floodproofed structures must be designed to withstand the expected maximum impact loads. Estimating the maximum force on the structure is complex because the force is influenced by the properties of the debris, particularly its mass, velocity, and orientation on impact, and the properties of the structure itself, especially its stiffness and inertia.

At present there is no one accepted approach for estimating debris impact loads. There are, in fact, three distinct—although, as we show, theoretically equivalent—approaches to estimating the maximum impact force. Each of these approaches estimates the maximum impact force based on the debris velocity and mass. All of the approaches are based on a one-degree-of-freedom system (i.e., only the mass of the debris is considered in the calculation of forces). The contact stiffness approach is based on a one-degree-of-freedom spring-mass system where the stiffness of the interaction between the "debris" and the structure is required. The American Association of State Highway Transportation Officials (AASHTO 1998) *LRFD Bridge Design Specifications* uses this approach to estimate the loads resulting from ship collisions with bridge piers. The impulse-momentum approach equates the momentum of the debris and the time history of force, or impulse, imparted on the structure. In this approach the stopping time of the debris and the shape of the force function with time must be assumed. This approach is used in the flood-proofing guidance provided by the Federal Emergency Management Agency (FEMA 1995) and the U.S. Army Corps of Engineers (1995). (For brevity we refer to these works collectively as FEMA guidance.) The work-energy approach equates the energy of the debris with the work done on the structure. This approach requires an estimate of the distance the structure moves from the time of the initial contact of the debris until the debris comes to rest. The National Association of Australian State Road Authorities (NAASRA 1990) *Highway Bridge Design Specification* guidance on designing bridges for debris impacts uses this approach.

The focus of this work was to obtain laboratory measurements of the forces caused by impacts of floating discrete woody objects (i.e., logs) on rigid structures. The tests also investigated the influence of collision geometry, determined by the debris orientation on impact, on the maximum impact forces. These data were then used to develop initial guidance for computing the maximum force associated with debris impacts.

Estimating Impact Forces

In the following section we develop a one-degree-of-freedom model of the impact between woody debris and a structure. We then discuss other influences that can affect the impact force: added mass and the debris orientation on impact. Finally, we review the guidance on impact forces. The guidance can be classified according to the governing assumptions made to estimate the maximum forces. The three basic approaches are: contact stiffness (AASHTO 1998); impulse momentum (FEMA 1995; U.S. Army Corps of Engineers 1995); and work energy (NAASRA

[1]Research Mechanical Engineer, Engineering Research and Development Center, U.S. Army Corps of Engineers, Hanover, NH 03755.

[2]Research Hydraulic Engineer, Engineering Research and Development Center, U.S. Army Corps of Engineers, Hanover, NH 03755. E-mail: steven.f.daly@erdc.usace.army.mil

Note. Discussion open until July 1, 2004. Separate discussions must be submitted for individual papers. To extend the closing date by one month, a written request must be filed with the ASCE Managing Editor. The manuscript for this paper was submitted for review and possible publication on September 17, 2002; approved on July 8, 2003. This paper is part of the ***Journal of Hydraulic Engineering***, Vol. 130, No. 2, February 1, 2004. ©ASCE, ISSN 0733-9429/2004/2-112–120/$18.00.

1990). The aim of each approach is to estimate the maximum impact force based on the velocity and mass of the woody debris. Each requires an additional parameter: impulse momentum requires the stopping time; work energy, the stopping distance; and contact stiffness, the effective contact stiffness. We discuss the assumptions required by each and show their equivalence.

One-Degree-of-Freedom Model

A log impacting a structure can be modeled as a one-degree-of-freedom system if the structure can be considered to be rigid. The descriptive equation of such a model is

$$(m_1+Cm_f)\ddot{x}+\hat{k}x=0 \tag{1}$$

where m_1=mass of the log; C=added mass coefficient; m_f=mass of the displaced fluid; and $\hat{k}$=effective contact stiffness of the collision.

It is reasonable to assume that the collision occurs over such a short duration that damping can be neglected. The effective stiffness of the collision is

$$\hat{k}^{-1}=\frac{1}{k_t}+\frac{1}{k_1} \tag{2}$$

where k_t=local stiffness of the structure at the impact zone; and k_1=elastic deformation of the log at impact. The structure will be rigid if the structure support stiffness is much greater than the stiffness of the target zone or the log. The structure will also act as if it is rigid if the mass of the structure is so great that it doesn't move appreciably in response to the impact of the log.

The variable x is the summation of the compression of the target face and the log during impact and rebound (e.g., $x=x_1+x_t$), and the dot notation indicates the time derivative of x. At the moment of contact between the debris and the structure (i.e., $t=0$), $x=0$ and $\dot{x}=u_1$, and the solution of Eq. (1) is

$$x=u\sqrt{\frac{(m_1+Cm_f)}{\hat{k}}}\sin\left(t\sqrt{\frac{\hat{k}}{(m_1+Cm_f)}}\right) \tag{3}$$

Given the linear relationship between the penetration depth and the normal force, $F=\hat{k}x$, the maximum impact force, $F_{i,\max}$, predicted using Eq. (3) is

$$F_{i,\max}=u_1\sqrt{\hat{k}(m_1+Cm_f)} \tag{4}$$

Thus, the maximum impact force is a function of the impact velocity multiplied by the square root of the product of the effective contact stiffness and the effective debris mass. Note that the maximum impact force is independent of the properties of the structure if the structure is rigid.

The value of C depends on the object's geometry, degree of submergence, orientation with respect to the direction of acceleration, and natural frequency. C approaches zero for a long slender object (e.g., a log) with its axis oriented with the direction of acceleration (Sarpkaya and Isaacson 1981). However, $C=1$ for the same object accelerated normal to its axis.

Several log sizes and geometries were used in this study, including short rectangular timbers and long, slender cylindrical logs. Estimates of the added mass coefficient for the geometries used in this study are given below. For small rectangular timbers with an impact angle of 0°, we assumed $C=0.22$; for full-size cylindrical logs with the same impact orientation, we assumed $C=0$. For the 90° impacts of the rectangular timbers, we assumed $C=2.4$ and 3.5 for square and rectangular timbers, respectively. For long cylindrical logs oriented 90° to the flow, we used $C=1$.

The effects of eccentricity and obliqueness of the impact can be included in the above analysis by augmenting Eq. (4)

$$F_{i,\max}=e\beta u_1\sqrt{\hat{k}(m_1+Cm_f)} \tag{5}$$

where e=reduction of the impact force as a result of eccentricity; and β=reduction of the impact force as a result of obliqueness. The reduction of the impact force as a result of eccentricity can be estimated using the analytic expression developed by Matskevitch (1997)

$$e=\frac{1}{\sqrt{1+\left(\frac{\varepsilon_0}{r_i}\right)\left(1+\mu\frac{r_0}{\varepsilon_0}\right)}} \tag{6}$$

where ε_0=distance from the center of gravity of the log to the point of impact; r_i=radius of gyration for the log; μ=coefficient of friction between the target and log; and r_0=radius of the log.

The reduction of the impact force as a result of obliqueness can be estimated simply as

$$\beta=\sin\phi \tag{7}$$

where ϕ=angle of the impact relative to the log surface.

Previous Approaches

In reviewing the previous approaches, we will not consider the reduction in impact force due to eccentricity or obliqueness, or the fluid added mass. These terms were not included in any of the previous analyses.

Eq. (4), which we refer to as the contact-stiffness approach, has the same form as the expression adopted for calculating vessel impact forces on bridge piers (AASHTO 1998), where the maximum collision force on the pier is based on the dead-weight tonnage of the vessel in long tons, and the vessel velocity is in feet per second.

The impulse-momentum approach equates the impulse acting on the debris in contact with the structure with the change in momentum of the debris. The governing equation for this approach is based on the definition of impulse I

$$I=\int F(t)dt=t_i\bar{F}_i=\int d(u_1m_1) \tag{8}$$

where F=force acting on the debris (a function of time, t); $\bar{F}_i$=time-averaged force; and I=total change in the momentum of the debris over the course of the impact.

Integration of Eq. (8) requires the functional relationship between impact force and time. If we assume that the momentum of the debris goes to zero as a result of the impact, then Eq. (8) becomes

$$\bar{F}_i=\frac{u_1m_1}{t_i}=\frac{u_1w_1}{gt_i} \tag{9}$$

where w=weight (=mg) of the debris; and g=gravitational constant. The impact duration, t_i, is equal to the time between the initial contact of the debris with the structure and the maximum impact force. An independent estimate of t_i is required to estimate the impact force. FEMA (1995) and the U.S. Army Corps of

Engineers (1995) have adopted the impulse-momentum approach. Eq. (9) is the expression used in the FEMA guidance, which suggests a value of 1 s for t_i.

A limitation of Eq. (9) is that it gives the average impact force, not the maximum force, an important point that is not explicitly stated in the FEMA (1995) guidance. An expression for the maximum force, $F_{i,\max}$, can be obtained if the function of the force with time, $F(t)$, is assumed. Based on Eq. (3) we would expect that the functional dependence of force with time is sinusoidal, thus

$$F_{i,\max}=\frac{\pi}{2}\frac{u_1 m_1}{t_i} \tag{10}$$

In the work-energy approach, the impact force is computed by equating the work done on the structure with the kinetic energy of the debris element and assuming that the velocity of the debris goes to zero as a result of the collision

$$W=\int F(x)\mathrm{d}x=\int \mathrm{d}\left(\frac{1}{2}mu^2\right) \tag{11}$$

where W=work done by the change in kinetic energy, $1/2mu^2$. The force is a linear function of the distance, x, over which it acts. We define S, the stopping distance of the debris, as the distance the debris travels from the point of contact with the target until the debris is fully stopped ($u=0$). Then Eq. (11) can be solved as follows:

$$\int_0^s kx\,\mathrm{d}x=\frac{1}{2}mu_0^2 \tag{12}$$

or

$$kS^2=mu_0^2 \tag{13}$$

Since $F_{i,\max}=kS$, Eq. (13) becomes

$$F_{i,\max}=\frac{mu_0^2}{S}=\frac{wu_0^2}{gS}$$

or

$$F_{i,\max}=\frac{2}{S}KE \tag{14}$$

This is the expression used by NAASRA (1990) to compute impact forces of woody debris on bridge piers. To estimate the maximum design impact load, NAASRA recommends a range of stopping distances based on the bridge design for a log with a minimum mass of 2 t (4,410 lbm). The stopping distances used in the NAASRA guidance vary with pier stiffness only, with shorter stopping distances for stiffer piers.

Though the above analyses of the maximum impact force are presented as three separate approaches, the one-degree-of-freedom model can be used to demonstrate that they are equivalent. We can use Eq. (3) to determine the values of t_i and S that coincide with $F_{i,\max}$. These are the values required by Eqs. (10) and (14)

$$t_i=\frac{\pi}{2}\sqrt{\frac{m_1}{k}} \tag{15}$$

and

$$S=u_1\sqrt{\frac{m_1}{k}} \tag{16}$$

Substituting Eq. (15) into Eq. (10) or Eq. (16) into Eq. (14) yields

$$F_{i,\max}=u_1\sqrt{km_1} \tag{17}$$

which is identical to Eq. (4) if the added mass coefficient is neglected.

Eqs. (15) and (16) show that impact duration and stopping distance are not constants that are independent of the properties of the logs involved in the collisions. Indeed, the impact duration depends on the debris mass and the contact stiffness of the interaction, while the stopping distance depends on the debris mass, the contact stiffness, and the approach velocity. Treatment of t_i and S as constants that are independent of debris mass and velocity has led to the disparate estimates of impact forces using these otherwise equivalent expressions. Given that all these approaches are equivalent if the functional relationships for stopping distance and impact duration are used, we have chosen to use the contact stiffness approach as the basis for analyzing the data in this study. This approach relies only on the effective contact stiffness, which for a first-order system is independent of log mass and velocity.

Experimental Procedures

All of the tests were conducted in the Cold Regions Research and Engineering Laboratory's Ice Engineering Facility. Tests using reduced-scale logs were conducted in the flume facility; tests using full-scale logs took place in the test basin. A complete description of the experiments can be found elsewhere (Haehnel and Daly 2002).

Flume Experiments

The flume allows tests that are hydrodynamically the same as conditions in the field, with the water and log moving and the target remaining stationary. The flume is capable of flows up to 0.25 m^3/s (4,000 gpm), and the bed slope can be varied to maintain a uniform flow depth. However, because the flume is small—1.22 m (4 ft) wide×0.61 m (2 ft) high×36.6 m (120 ft) long—only small (reduced-scale) logs could be used.

Logs of varying weight were used to measure the impact forces on a stationary load frame placed in the flow. The load frame had a rounded target mounted on a front plate, which in turn was mounted on three load cells that were fastened to a rigid frame mounted on the flume floor. The rounded target kept the point of impact concentrated between the three load cells, assuring that all of the load cells were in compression on impact. Three 8,900 N (2,000 lbf) load cells were used.

In the flume tests (Test Series 1) we varied log mass, flow velocity, and impact orientation. Table 1 shows the levels for each of the factors studied in these experiments. The convention used for impact orientation was that 0° indicated a log with its long axis parallel to the flow (head-on impact) and 90° indicated a log aligned perpendicular to the flow (broad-side impact). The logs for the flume tests were cut from stock pressure-treated lumber (rectangular cross section).

The logs were released into the flow 7.6 m (25 ft) upstream of the load frame. This was a sufficient distance for the log to accelerate to the flow velocity before impact. Care was taken to ensure that the impacts were within a few degrees of the intended impact angle and that the logs struck the center of the target. If this was not the case, the test was repeated.

Table 1. Test Matrix for Flume Experiments Series 1; Each Factor was Tested against All Other Factors with Three Replicates for Each Test, Giving Total of 144 Tests

Target material	Impact orientation (deg)	Log: Actual mass kg (lbm)	Log: Dimensions, cm (in.)	Actual average impact velocity, m/s (ft/s)
Wood	0	5.90 (13.0)	8.9×14×91 (3.5×5.5×36)	0.381 (1.25)
Steel	90	12.0 (26.5)	14×14×91 (5.5×5.5×36)	0.533 (1.75)
		14.4 (31.8)	14×19×91 (5.5×7.5×36)	0.800 (2.62)
	—	19.7 (43.5)	19×19×91 (7.5×7.5×36)	—

Basin Experiments

The test basin is 9.1 m (30 ft) wide×37 m (120 ft) long×2.4 m (8 ft) deep and can easily accommodate logs that are prototype size. However, the water is stationary in the basin. For these tests we placed the log in the stationary water and mounted the target on the movable test carriage. This allowed us to ram the log with the target. The load frame used in the basin was similar to that used in the flume. The same rounded target and front plate were used in both the basin and the flume. However, we mounted two 8.9 kN (2,000 lbf) load cells on the top of the front plate and one 22 kN (5,000 lbf) load cell on the bottom to allow measurement of the larger loads anticipated in the basin tests. The load cells were fastened to a flexible frame that was in turn mounted on the underside of the test carriage. Substituting plates of varying thickness for the "end plates" varied the stiffness of the load frame. To make the frame extremely stiff, an additional longitudinal stiffener was added that extended between the two end plates.

Test Series 3

To confirm that the experiments in the flume and test basin would produce equivalent results, we ran a direct comparison with the flume tests by repeating the tests conducted with the 19.7 kg (19×19×91 cm) log in the test basin. Table 2 shows the test matrix for these experiments. Three replicates were performed at each level.

Test Series 4

This test series used full-scale red pine logs in the test basin. Table 3 gives the test matrix for these experiments. These logs were 24–32 cm in diameter and 4.6–8.5 m long. The FEMA (1995) guidance gives a design log mass of 454 kg. We could not accommodate a log this large in the test basin; the maximum log mass used in these tests was 330 kg. The weight of the logs varied with the time they spent in the water. The logs were weighed at the beginning and end of each test day to determine the average weight for the associated tests. The range in weight of logs used was 171–330 kg. Tests were conducted at 0 and 90° orientations for a variety of impact velocities and two structural stiffnesses.

To control the impact orientation the logs were held in position with ropes that extended to the edges of the test basin. At the basin walls, 2.3–4.5 kg weights were placed on the ropes to hold them in place until impact. At impact the ropes pulled free, allowing the log to move freely in the water. One end of the log was rounded in the horizontal direction. Since the target was also rounded yet oriented in the vertical direction, the impact zone was essentially reduced to a point for 0° impacts. Furthermore, since the logs were round, any impact other than 0° was also at a point.

Table 2. Test Matrix for Basin–Flume Comparison Experiments (Test Series 3)

Impact velocity, m/s (ft/s)	Target material	Impact orientation (deg)
0.381 (1.25)	Steel	0
0.800 (2.62)	Steel	0
0.381 (1.25)	Wood	0
0.800 (2.62)	Wood	0
0.381 (1.25)	Steel	90
0.800 (2.62)	Steel	90
0.381 (1.25)	Wood	90
0.800 (2.62)	Wood	90

Table 3. Test Plan for Basin Full-Scale Tests [This Shows Plan for Only one Series of Full-Scale Tests]

Impact orientation (deg)	Impact velocity m/s (ft/s)	Target frame stiffness (MN/m)	Log butt diameter cm (in.)	Replicates
0	0.076 (0.25)	32.1	25 (10)	1
		32.1	30 (12)	1
	0.15 (0.5)	32.1	25 (10)	1
		32.1	30 (12)	1
	0.30 (1)	21.8	25 (10)	1
		21.8	30 (12)	1
		32.1	30 (12)	1
	0.61 (2)	21.8	25 (10)	2
		21.8	30 (12)	2
		32.1	25 (10)	2
		32.1	30 (12)	2
	0.91 (3)	21.8	25 (10)	2
		21.8	30 (12)	2
	1.2 (4)	21.8	25 (10)	2
		21.8	30 (12)	2
		32.1	25 (10)	2
		32.1	30 (12)	2
	1.5 (5)	21.8	30 (12)	1
	1.8 (6)	21.8	30 (12)	1
90	0.61 (2)	21.8	25 (10)	2
		21.8	30 (12)	2
		32.1	25 (10)	2
		32.1	30 (12)	2
	1.2 (4)	21.8	25 (10)	2
		21.8	30 (12)	2
		32.1	25 (10)	2
		32.1	30 (12)	2

Note: Series 4: Log mass, velocity and impact orientation; log length =8.53 m (28 ft), load frame weight=127 kg; eccentricity=0, and target =steel.

Test Series 5

Using various end plates and the longitudinal stiffener, we were able to vary the stiffness of the test structure in the test basin from 0.607 to 120.0 MN/m, a factor of 200. Mounting lead weights on the bottom plate of the flexible frame varied the inertia of the frame. We could add up to 187 kg to the frame, more than doubling the inertia of the load frame. We conducted tests using a full-scale log (8.53 m long×25 cm butt diameter) at 0° orientation for impact velocities of 0.15, 0.30, and 0.61 m/s, structural stiffnesses of 0.607 and 120.0 MN/m, and structural inertias of 127 and 314 kg. Three replicates were conducted for each test.

Test Series 7 and 8

In Test Series 7, Oblique Impacts, we varied the orientation of the debris impact from 0 to 90° in 10° increments. The eccentricity was 0 for all these tests. In Test Series 8, Eccentric Impacts, we varied the eccentricity of the impacts by varying the impact location along the long axis of the log in 0.305 m increments. All the impacts in Test Series 8 were carried out at an orientation of 90°. In both Test Series 7 and 8 a full-scale log was used, all tests were carried out at a single velocity of 1.2 m/s, and we conducted these tests using the stiffest test structure (120 MN/m). Three replicates were conducted for each test.

Results and Discussion

Maximum Impact Force

The relevant experimental results described above can be used to test the utility of using the contact stiffness approach for computing debris impact forces. The data that we will use are those generated by Test Series 1, 3, and 4. Tests were conducted at 0 and 90° orientations for a variety of impact velocities using reduced-scale logs in the flume and full-scale logs in the test basin. The complete time history of force was recorded for each test, along with the velocity and mass of the logs. The initial peak in the force record was selected as the maximum impact force. In the analysis below, the fluid added mass is included in computing the log mass.

Three observations of the data are in order. First, the data that exhibit the most scatter are the reduced-scale impact tests conducted in the flume. Based on our observations during the tests, it is likely that the scatter in the flume data reflects the difficulty in controlling the exact impact geometry with an object moving with the flow. Slightly eccentric and oblique impacts were the rule rather than the exception in the flume tests, and the scatter in the data reflects the resulting reduction in forces. In Test Series 1 the exact orientation of the log at the time was not recorded, only the intended orientation of 0 or 90°. Second, the full-scale tests in the test basin recorded in Test Series 4 at an orientation of 90° and experiencing an impact at the midpoint of the log displayed a markedly lower maximum impact force than would be expected. The explanation for this reduction is undoubtedly flexure of the logs during impact. The large size of the logs allowed them to flex between their midpoint and their ends. The logs were therefore not accelerated uniformly along their length during an impact. And third, the reduced-scale tests in the flume and the reduced-scale tests in the test basin conducted in Test Series 3 produced similar and compatible results.

A short discussion is necessary regarding the applicability of a one-degree-of-freedom model to the laboratory measurements. A one-degree-of-freedom model is the basis of the three approaches currently used for computing debris and vessel impact forces. As stated earlier, it requires that the structure be rigid, that is, not move significantly during impact. This lack of movement can result either because the structure is much stiffer than the impacting debris or because the structure is massive and the debris rebounds off the surface of the structure before the structure moves appreciably. It is important that the laboratory data were collected under conditions that simulate a one-degree-of-freedom situation. The obvious means of assuring this was to ensure that the measured stiffness of the structure was much greater than the stiffness of a log. The actual stiffness of the laboratory structures was estimated through measurement of the natural frequency of the structures and through measurements of the structure displacement under static loads. The two estimates provided similar results. Surprisingly, however, it is not straightforward to estimate the stiffness of the wooden logs during the brief durations of impacts. The stiffness of the collision between the log and the structure is determined by the exact geometry of the impact zone of the log and the structure, the definition of which is beyond the scope of this study. An alternative means of assuring that the measurements are made under one-degree-of-freedom conditions is to successively increase the stiffness of the structure until the maximum impact forces reach a constant level that does not change with further increases in the structure stiffness. This process was conducted in Test Series 5, and the results are shown in Fig. 1. It can be seen that the linear envelope containing the test results coincides with the data collected using a structure with a stiffness of 22 MN/m and that further increases in the structure stiffness to 120 MN/m did not increase the maximum impact forces. The square of the slope of the line that defines the linear envelope or upper bound of the data provides an estimate of the upper limit of the effective contact stiffness of the collision; using this approach we found that the effective contact stiffness for woody debris striking a rigid structure is approximately 1.1–2.4 MN/m. This suggests that a structure can be considered to be rigid if the structure stiffness is at least ten times the effective contact stiffness. All of our data (except for Test Series 5) were collected using structures with a stiffness of 22 MN/m or greater, indicating that a one-degree-of-freedom model should be applicable.

The measured maximum impact forces are plotted against the "augmented" velocity to evaluate the contact-stiffness approach (Fig. 2) using data from Test Series 1, 3, and 4. The augmented velocity is $u\sqrt{m}$, where u is the velocity of the log and m includes the fluid added mass, if appropriate. It can be seen that a linear envelope would contain all the data, and the maximum impact force is, in Newtons

$$F_{i,\max} = 1550u\sqrt{m} \tag{18}$$

where u=velocity (m/s) and m=mass (kg). Thus, Eq. (18) is equivalent to using Eq. (4) with $\hat{k}=2.4$ MN/m and provides a slightly conservative prediction of the impact force over the full range of data measured in this study (Fig. 3).

As stated, Eq. (18) represents the upper bound of the data. There is notably a grouping of data, specifically the flume data, that lies close to the line represented by Eq. (18) (Fig. 1), but slightly below it. There are two reasons that the flume data lie below this line. First, the high occurrence of slightly oblique or eccentric strikes in the flume experiments increased the scatter in the data and has the effect of reducing the impact force, as previously discussed. Second, the stiffness of the load frame used in the flume was never measured in these experiments and therefore is not known. Yet the upper limit of these flume data provides a

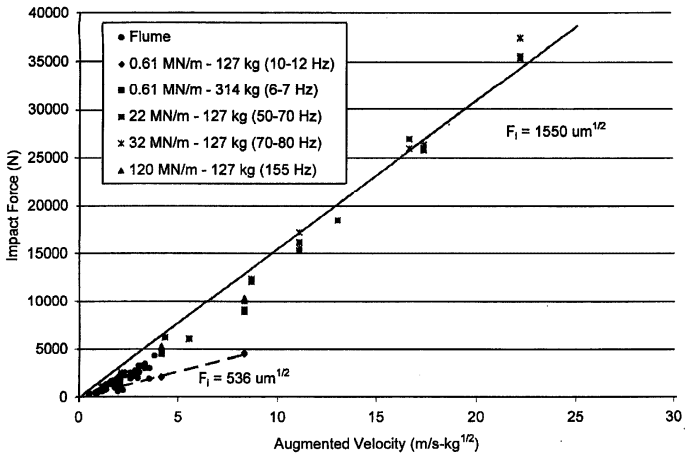

Fig. 1. Effects of structure stiffness and mass on impact force (test series 1, 4, and 5); only 0° impacts are shown

constant of approximately 1,070 for Eq. (18), which is somewhat less than the bounding envelope given by Eq. (18). This suggests that the effective contact stiffness in the flume experiments may have been slightly lower than that measured in the basin experiments (on the order of 1.1 MN/m). As a consequence, using the bounding envelope for all of the measured data to determine the effective stiffness tends to slightly overpredict the impact forces for measured forces below 10 kN (Fig. 3), the majority of which were measured in the flume. Thus, using an effective contact stiffness of 2.4 MN/m is a reasonable (yet slightly conservative) estimate of the contact stiffness for collisions of woody debris with a rigid structure over the range of data we obtained in this study. This is a reasonable result, considering that the effective contact stiffness used in the AASHTO guidance for vessel impacts on bridge piers is within this same order of magnitude: 14 MN/m (AASHTO 1998).

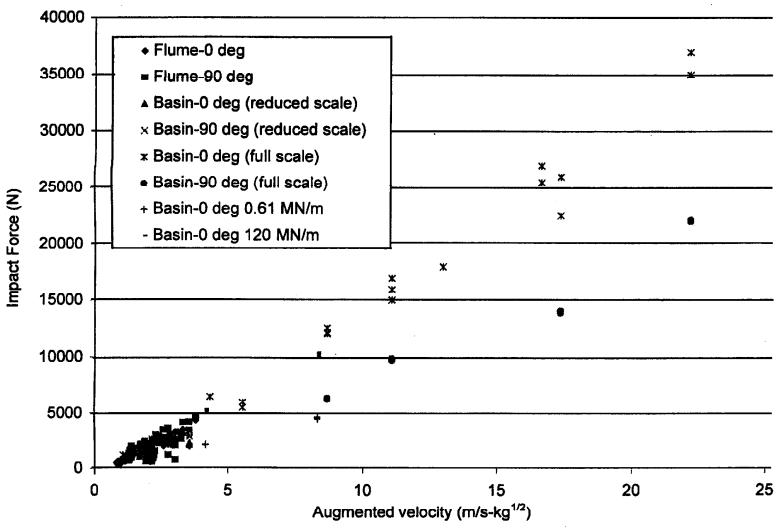

Fig. 2. Contact-stiffness approach applied to laboratory data [test series 1 (flume), 3, and 4 (basin)]; added mass is included for 90° impacts

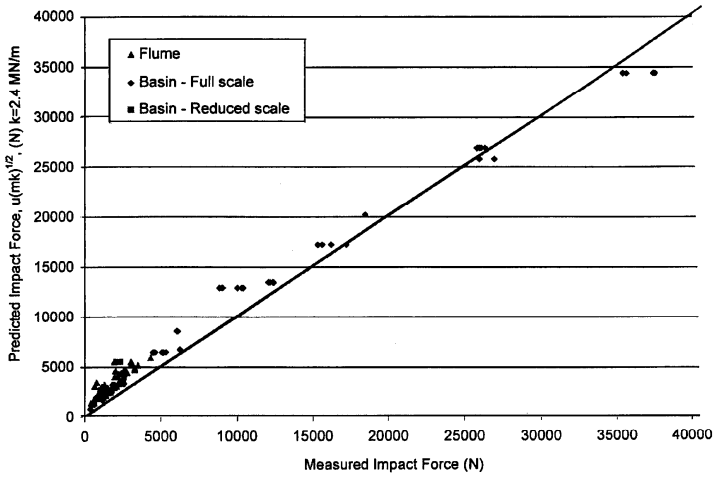

Fig. 3. Predicted versus measured values of impact force using contact-stiffness approach [Eq. (16)], data are for 0° impact orientation

Debris Orientation on Impact

In all of the tests discussed above, the debris impacted the structure at an angle of 0 or 90° to the axis of the logs, and the line of impact passed through the center of gravity of the logs. We collected laboratory data in Test Series 7 and 8 to evaluate the reduction in impact load that could be expected when the impacts were at an oblique angle or eccentric. We investigated each separately. We increased the eccentricity while keeping the impact on the structure perpendicular to its long axis (no obliqueness) to evaluate the effect of eccentricity. We also increased the obliqueness of the impacts while impacting the structure at its midpoint so that the line of impact passed through the center of gravity of the logs. In general, we found that the maximum impact force decreased in a consistent manner as the eccentricity or obliqueness of the impact increased.

Figs. 4 and 5 display the effects of eccentricity and obliqueness, respectively, on the maximum impact force. In these plots the measured maximum impact force has been normalized by $F^{90}_{i,\max}$, the maximum impact force for a central impact with a log orientation of 90°. For the eccentric impacts in Fig. 4, the impact

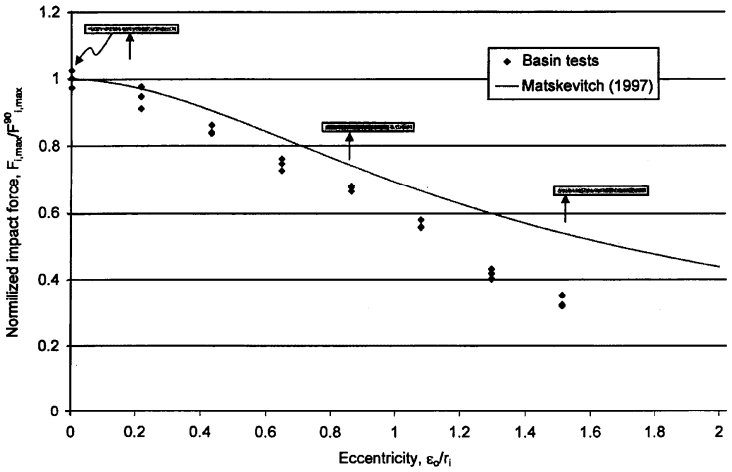

Fig. 4. Effects of impact eccentricity on force; log used was 4.9 m (16 ft) long and weighed 171 kg (378 lbm); diagrams show impact geometry

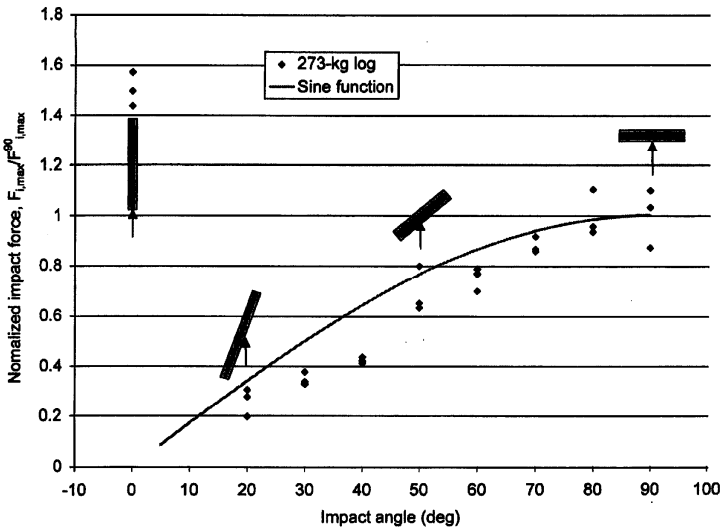

Fig. 5. Effects of impact orientation on force; the log used was 8.08 m (26.5 ft) long and weighed 93.4 kg (206 lbm); diagrams show impact orientation

location is expressed as a normalized distance, where ε_0 is the distance from the center of the log and r_i is the radius of gyration for the log. We also display Matskevitch's (1997) estimate of the decrease in the maximum impact force with increasing eccentricity. His estimate provides a reasonable fit to the data, although the measured data show a more rapid decrease in the maximum impact force with eccentricity. We suspect that flexure of the logs, which is not accounted for in Matskevitch's formula, accounts for this discrepancy.

Fig. 5 displays the effects of oblique impacts on the maximum impact force. There is a decrease as the impact angle decreases from 90 to 20° that correlates well with the sine of the angle, as might be expected (20° was the smallest angle that could be discerned for the oblique impacts, although impacts occurred at smaller angles). Collisions at angles between 0 and 20° directed most of the force toward the edge of the target, putting one or more of the load cells into tension. The force rose abruptly at an impact angle of 0°, as would be expected, as the impact at this orientation was no longer oblique.

Conclusions

We developed a one-degree-of-freedom model to describe impact forces between woody debris and a rigid structure. The maximum impact force is a function of the impact velocity (the relative velocity between the debris and structure), the mass of the debris, and the effective stiffness of the collision between the object and structure. It is independent of the properties of the structure if the structure is considered to be rigid. The added mass of the water and the eccentricity and obliqueness of the collision also affect the maximum impact load.

We reviewed the three approaches that represent the existing guidance on design for impact loads: impulse momentum (FEMA 1995); work-energy (NAASRA 1990); and contact stiffness (AASHTO 1998). Each of these approaches estimates the maximum impact force based on the debris velocity and mass. Each requires that an additional parameter be specified: the stopping time for the impulse-momentum approach; the stopping distance for the work-energy approach; and the effective contact stiffness of the collision for the contact-stiffness approach. We show that all three approaches can be derived from a single-degree-of-freedom model of the collision and are equivalent. We show that neither stopping time, in the case of impulse momentum, nor stopping distance, in the case of work energy, is an independent parameter. Stopping time depends on the effective contact stiffness and the debris mass; stopping distance depends on the effective contact stiffness, the debris mass, and the debris velocity.

Based on the laboratory data, we estimate that the effective contact stiffness of the collision varies over a narrow range (1.1–2.4 MN/m); 2.4 MN/m is a good upper-bound estimate and can be used in the contact-stiffness approach over a wide range of debris mass and velocity. It is problematic to select a single value for stopping time or stopping distance that can be applied over a wide range of debris mass and impact velocity. We could improve the ability of the impulse-momentum and work-energy approaches to reproduce the laboratory results by making the stopping time or stopping distance variable rather than constants. But then both approaches will be identical with the contact-stiffness approach.

Impact geometry has a significant effect on the maximum impact force. Though added mass considerations would suggest that peak forces should occur for a 90° central impact (broad-side impact), it appears that flexure of the long, slender log upon impact reduces the force significantly. We found that the peak impact force is associated with the log striking the target on its end (with the long axis of the log parallel to the flow direction and normal to the target face). In this orientation the added mass effects are negligible, and the mass of the log can be used directly to compute the impact force. Eccentric and oblique impacts sys-

tematically reduce the maximum impact force as each is increased. The effects of eccentricity can be estimated using the formula of Matskevitch (1997). The effects of obliqueness are proportional to the sine of the angle of impact.

Regardless of the approach used to estimate the maximum impact force, the data demonstrate that a log striking a rigid structure with its end (with the long axis of the log parallel to the flow direction and normal to the structure face, i.e., 0° collisions) produces the maximum impact force. In this orientation, added mass is negligible, and the mass of the log can be used directly to compute the maximum impact force.

Acknowledgments

The Federal Emergency Management Agency funded this work. The writers thank Thomas McLane and Lorena Dias of the American Society of Civil Engineers and Dr. David Kriebel of the U.S. Naval Academy for their support in executing this work. This work could not have been accomplished without the technical assistance of Michael Walsh, Dennis Lambert, Dr. Devinder Sodhi, John Gagnon, Gordon Gooch, and Charles Clark.

References

American Association of State Highways and Transportation Officials (AASHTO). (1998). "LRFD bridge design specifications." 2nd Ed., Washington, D.C., 26–27.

Federal Emergency Management Agency (FEMA). (1995). "Engineering principles and practices for retrofitting floodprone residential buildings." *FEMA Rep. No. 259*, Washington, D.C.

Haehnel, R. B., and Daly, S. F. (2002). "Maximum impact force of woody debris on floodplain structures." *Rep. No. ERDC/CRREL TR-02-2*, USA Cold Regions Research and Engineering Laboratory, Engineering Research and Development Center, Hanover, N.H. ⟨http://www.crrel.usace.army.mil.techpub/CRREL Reports/reports/TR02-2.pdf⟩.

Matskevitch, D. G. (1997). "Eccentric impact of an ice feature: Linearized model." *Cold Regions Sci. Technol.*, 25, 159–171.

National Association of Australian State Road Authorities (NAASRA). (1990). "Highway bridge design specification."

Sarpkaya, T., and Isaacson, M. (1981). *Mechanics of wave forces on offshore structures*, Van Nostrand–Rienhold, New York.

U.S. Army Corps of Engineers. (1995). "Flood-proofing regulations." *Engineering Pamphlet 1165-2-314*, Washington, D.C.

２．コメント回答②（電力中央研究所の実験における車両の軸剛性の同定において，付加質量が含まれていることの詳細を示すこと。）

Haehnel and Daly（2004）に記載されている$F = v\sqrt{km}$は，電力中央研究所（2015）※1及び高畠ら※2が実験における実現象を再現する車両（全長 3295㎜，全幅 1395㎜，全高 1475㎜）の有効軸剛性を同定するのに用いられている式である。車両の有効軸剛性は，実際の自動車を用いた静的載荷実験及び衝突実験（気中衝突実験，水流中衝突実験）を実施し，構造形式や破壊過程に基づいた軸剛性を取得している。水流中衝突実験では，衝突荷重を測定し，漂流物の質量 m は車両の質量で一定とした上で，その荷重を$F = v\sqrt{km}$で再現するように軸剛性 k を求めている。車両の水流中衝突実験状況を図－１に示す。

以降に，高畠ら※2における記載を示す。

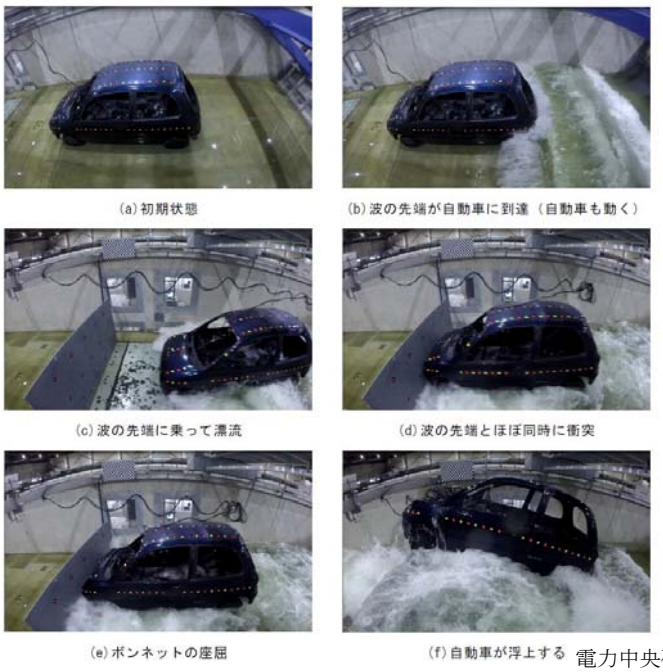

電力中央研究所（2015）より

図－1　車両の水流中衝突実験状況

土木学会論文集B2(海岸工学), Vol. 71, No. 2, I_1015-I_1020, 2015.

津波漂流物の衝突力推定における軸剛性モデル

高畠　大輔[1]・木原　直人[2]・宮川　義範[2]・
甲斐田　秀樹[2]・柴山　淳[3]・池野　正明[4]

[1]正会員　電力中央研究所　地球工学研究所　(〒270-1194 千葉県我孫子市我孫子1646)
E-mail:tdaisuke@criepi.denken.or.jp
[2]正会員　電力中央研究所　地球工学研究所　(〒270-1194 千葉県我孫子市我孫子1646)
[3]非会員　電力中央研究所　地球工学研究所　(〒270-1194 千葉県我孫子市我孫子1646)
[4]正会員　電力中央研究所　環境科学研究所　(〒270-1194 千葉県我孫子市我孫子1646)

津波漂流物の衝突力評価においては，漂流物の質量，衝突速度に加え，漂流物の構造形式に応じた軸剛性の設定が必要になる．しかし，軸剛性の設定値やそのモデル化方法は明らかになっていない．本論文では，実物の自動車を用いた静的載荷実験と気中・水流中衝突実験を実施し，軸剛性のモデル化を行うとともに，既往の衝突力推定式における適用性について検討した．実験に用いた軽自動車の軸剛性は，衝突速度に応じて変化する多段階のモデルによって表現できることを明らかにした．さらに，衝突実験結果と既往式による推定結果の比較から，衝突速度に応じた軸剛性を用いることにより，合理的かつ簡易的に衝突力が評価可能であることを確認した．

Key Words : *tsunami, floating debris, impact force, axial stiffness, large scale experiment*

1. はじめに

津波に起因する構造物の損傷原因の一つとして，船舶や自動車などの津波漂流物による衝突が挙げられる．その影響評価方法として，衝突時に生じる衝突力を推定する方法が考えられる．津波漂流物による衝突力に関しては，数々の推定式が提案されており，これらの多くは，漂流物（以下，衝突体）の「質量」，「衝突速度」，「剛性または弾性率」を入力することにより衝突力が得られる．例えば，松冨[1]や有川ら[2]の提案式は，木材やコンクリートブロックの衝突を想定しており，「剛性または弾性率」として衝突体の材料物性値が入力される．一方で，FEMA(2012)[3]ではHaehnel and Daly[4]によって提案された次式を採用しており，ここでは，「剛性または弾性率」として衝突体の材料物性と構造形式を考慮した軸剛性が入力される．

$$F = v\sqrt{\hat{k}\left(m_a + m_f c\right)} \tag{1}$$

$$\frac{1}{\hat{k}} = \frac{1}{k_t} + \frac{1}{k_a} \tag{2}$$

ここに，Fは衝突力[N]，vは衝突速度[m/s]，m_aは衝突体の質量[kg]，m_fは衝突体によって押し退けられた流体の質量[kg]，cは付加質量係数，k_a及びk_tはそれぞれ衝突体，被衝突体の軸剛性[N/m]であり，上付き文字「^」はこれらを考慮した衝突時の等価な軸剛性である．ここで，軸剛性は，ある構造体の軸方向の荷重増分量を変位増分量で除した値で定義される．津波漂流物として，船舶や自動車を考慮する場合は，これらの構造形式に応じた軸剛性の設定が必要になる．しかしながら，これらの軸剛性については，そのモデル化や数値が明らかではない．

本研究では，実物の自動車を用いた静的載荷実験及び衝突実験を実施し，軸剛性のモデル化と既往推定式への適用性を検討した．さらに，漂流物として想定される自動車や船舶の軸剛性を収集した．

2. 実験方法

本研究では，静的載荷実験，気中衝突実験，水流中衝突実験の順に実験を実施した．自動車の寸法は，全長3295mm，全幅1395mm，全高1475mmである．また，衝突実験中に飛散の可能性のあるガラス窓や漏油の危険性のある機械類は，静的載荷実験前に予め除いた．ただし，以下の議論で対象とする軸剛性には影響を与えない．その結果，車体の総質量は316kgとなった．尚，全ての実験で同一の自動車を用いた．以下に，それぞれの実験方法を示す．尚，実験の詳細は文献5)を参照されたい．

(1) 静的載荷実験

静的載荷実験では，自動車の荷重-変位関係を取得し，軸剛性を把握した．実験装置を**図-1**に示す．本論文では，前面衝突を想定し，載荷方向を自動車の水平長手方向とした．そして，自動車をコンクリート反力壁とリニアローラーに積載した載荷板の間に設置し，載荷板の後方に固定した200kN油圧ジャッキを用いて載荷した．尚，ジャッキはコンクリート反力床に固定された鋼製重錘と載荷板の間に固定し，ジャッキが鋼製重錘を押す反力を自動車への荷重とした．ただし，荷重のオーダーが小さいため，ジャッキ先端にバネを取付け，接触式変位計（東京測器製：CPD-50）でバネの縮み量を計測し，バネ定数を乗じ反力を求めた．一方，自動車の変位は，載荷板の変位を接触式変位計（東京測器製：CPD-100）で計測した．ただし，「水流中衝突実験前に自動車に残留変形を生じさせない」という制約の下，1.2kN以下の低載荷とし，0kNと1.2kNの間で増減を3回繰り返した．

(2) 衝突実験

気中及び水流中で衝突実験を実施し，衝突速度と衝突力の関係を取得した．衝突実験は電力中央研究所の津波・氾濫流水路[9]（以下，水路）内で実施した．衝突実験で計測された衝突力，衝突速度の範囲及び実験回数を**表-1**，概略図を**図-2**に示す．自動車の初期位置は，**図-2**に破線で示すように，気中実験では自動車の先端が鋼板から500mm程度離れた位置，水流中実験では7000mm程度離れた位置とした．被衝突体には横3000mm，高さ1500mm，厚さ19mmの鋼板と直径20mm，長さ100mmの鋼棒40本及び固定治具で構成された反力壁を用いており，衝突時に鋼棒に発生するひずみをひずみゲージ（共和電業製：KFG-2-120）により計測し衝突力に換算した．また，3台のカメラ（解像度：640×480pixel）を用いて，画像解析により計算される時々刻々の自動車の3次元座標値から衝突速度を取得した．気中実験では，「水流中実験前に自動車に残留変形を生じさせない」という制約の下，人力で自動車を押し，0.4m/s以下の低速度衝突とした．一方，水流中実験では，水路内初期水深（0mm，200mm），ゲートを隔てた上流側貯水深（1300mm，1700mm，2000mm）をパラメタとした6種の流れにより自動車を衝突させた．尚，最大衝突速度は実規模相当の3.9m/sである．**表-2**に，漂流物なしの条件で計測した流れの最大流速・浸水深を示す．ただし，試験No.6で用いた流れの条件に対する流れの計測は実施していない．

表-1 衝突実験ケース

	気中	水流中
衝突力[kN]	0.8～2.9	24.6～86.1
衝突速度[m/s]	0.26～0.38	0.9～3.9
実験回数	24	6

表-2 流れの条件

試験No.	設定値[mm]		計測値	
	ユニット	水路	流速[m/s]	浸水深[m]
1	2000	200	3.38	2.05
2	1300	200	2.64	1.17
3	1300	0	5.36	2.19
4	1700	0	5.62	1.90
5	2000	0	6.02	2.43
6	1700	200	※流れの計測を実施せず	

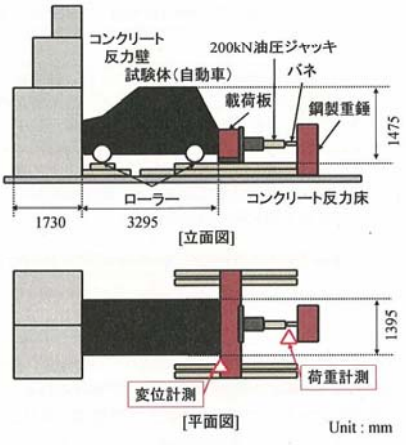

図-1 静的載荷実験の実験装置

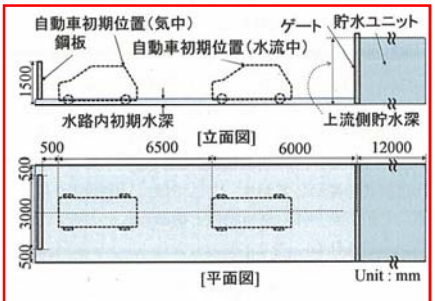

図-2 衝突実験の概略図

3. 軸剛性モデルによる衝突力推定手法

(1) 実験結果に基づく軸剛性のモデル化

a) 静的載荷実験結果に基づく軸剛性のモデル化

図-3に静的載荷実験から得られる荷重-変位関係を示す．処女載荷曲線に着目すると，下に凸となっており，変位17mmまでは抵抗が小さい．また，除荷軌道は処女載荷時の軌道と異なり，ほぼ変位の減少を伴わない急激な荷重低下を示した．これは，自動車の各パーツの接合部における隙間の解消により非弾性変形が生じたものと

考えられる．次に処女載荷曲線を対象に軸剛性の変化に着目する．載荷直後は軸剛性がほぼ0であり，変位17mm，変位21mmにおいて軸剛性が増加している．作用する荷重レベルにより軸剛性が変化していることから，衝突荷重や衝突速度によって変化する多段階の剛性域で軸剛性をモデル化できるものと考えられる．ここでは，変位17mm前後の軸剛性の変化は，変位21mm前後のそれに比べて十分小さいため，変位0mmから21mmまでを1つの軸剛性域とみなし，変位21mm以前の軸剛性域を1次剛性域，それ以降を2次剛性域と定義する．

b) 衝突実験結果に基づく軸剛性のモデル化

図-4に水流中実験1回目における衝突力の時系列変化を示す．衝突直後から衝突力が緩やかに増加し始め，0.07sec付近において急増し，その後0.09sec付近において極大荷重となる．**図-5**に水流中実験1回目終了後の試験体前部の様子を示す．自動車前面にはウレタン製バンパーが取付けられているが，それを支持するバンパービーム（以下，ビーム）やその後方に位置するフロントサイドメンバー（以下，メンバー）に残留変形が確認できる．一般に自動車の前突時には，まずメンバーやクラッシュボックスが軸圧縮荷重に抵抗する．次に，これらが軸方向座屈すると，後方のエンジンやフロントサイドエクステンション等で荷重に抵抗する（**図-6**[7]参照）．また，バンパーやビームの主たる役割は，衝突時の衝撃吸収であり，主に荷重に抵抗する部材ではないため，メンバーに比べて剛性が低い．以上の自動車構造を勘案すると，バンパーやビームに残留変形が発生していない静的載荷実験や気中実験では，これらにより衝撃を十分に吸収できる荷重レベルであり，バンパーやビームが荷重に抵抗可能であったと考えられる．一方，水流中実験1回目においても，衝突直後はバンパーやビームが荷重に抵抗していたが，0.07sec付近でこれらの抵抗力が低下・喪失したため，以降では，メンバーにより荷重に抵抗し，最終的に座屈により荷重が低下したと推測される．従って，**図-7**に示すように，バンパーやビームにより荷重に抵抗する1次及び2次，メンバーにより荷重に抵抗する3次の3つの剛性域で，軸剛性がモデル化できると考えられる．

次に衝突直前の運動エネルギーと衝突による変形で吸収されるエネルギーが等しいと仮定し，以下の手順で3次軸剛性k_3を算出する．すなわち，①**図-4**より2次軸剛性域の最大荷重とその後に発生する極大荷重（**図-7**におけるf_2とf_3）を読み取る，②自動車質量と衝突速度より衝突直前の運動エネルギーを算出する，③吸収エネルギー（**図-7**における多角形O-A-B-C-Dで囲まれる領域の面積）を3次軸剛性で表し，運動エネルギーと等価として軸剛性を定める．以上より算出される各剛性域の軸剛性，荷重範囲，速度範囲を**表-3**に示す．ただし，3次剛性域に関しては，その上限値を水流中実験で計測された最大値としている．衝突荷重または衝突速度に依存して，軸剛性が急激に変化することが理解できる．

表-3 各剛性域の軸剛性，荷重範囲，速度範囲

剛性域	軸剛性[kN/m]	荷重範囲[kN]	速度範囲[m/s]
1次	6.25×10^{0}	0～0.13	0～0.09
2次	1.18×10^{2}	0.13～12.5	0.09～2.04
3次	2.04×10^{3}	12.5～(86.1)	2.04～(3.90)

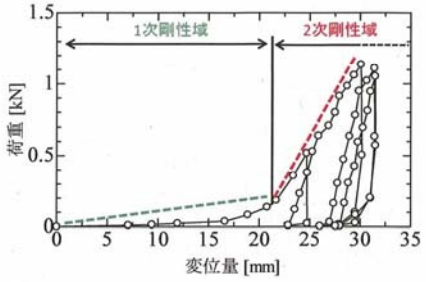

図-3 荷重-変位関係（静的載荷実験）

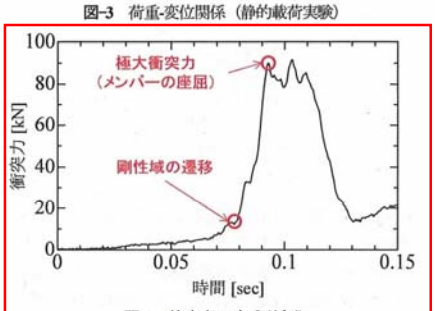

図-4 衝突力の時系列変化

図-5 ビーム・メンバーの残留変形の様子

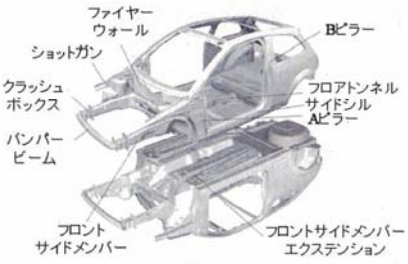

図-6 車体構造[7]

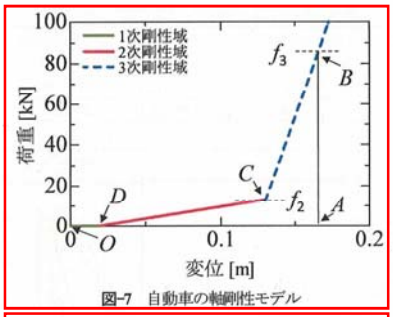

図-7 自動車の軸剛性モデル

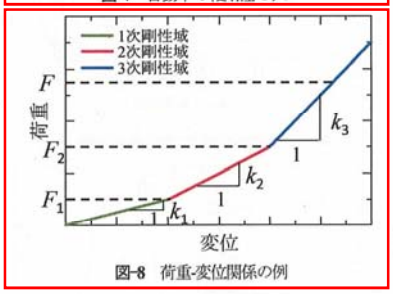

図-8 荷重-変位関係の例

(2) 既往推定式を利用した衝突力推定手法

図-8に示すような荷重-変位関係を持つ衝突体を想定し，前述のように，衝突直前の運動エネルギーと衝突エネルギーが等価と仮定する．この時，運動エネルギーと吸収エネルギーの関係は図中の記号を用い，次式となる．

$$\frac{1}{2}mv^2 = \frac{1}{2}\frac{F_1^2}{k_1} + \frac{1}{2}\frac{F_2^2 - F_1^2}{k_2} + \frac{1}{2}\frac{F^2 - F_2^2}{k_3} \quad (3)$$

ここに，mは衝突体の質量[kg]，vは衝突速度[m/s]，Fは衝突力[N]，kは軸剛性[N/m]で，下付き文字iはそれぞれ剛性域iの値であることを示す．式(3)の右辺の各項は，各剛性域の吸収エネルギーで記述されるため，式(3)は容易にn段階のモデルに拡張できる．式(3)をn(≧2)段階に拡張しFについて整理すると次式になる．

$$F = v\sqrt{k_n m}\sqrt{1 + \frac{1}{mv^2}\left(\sum_{i=1}^{n-1} F_i^2\left(-\frac{1}{k_i} + \frac{1}{k_{i+1}}\right)\right)} \quad (v_{n-1} \le v \le v_n) \quad (4)$$

ここでv_nはn次剛性域の最大速度であり，式(4)はn次剛性域の荷重-速度関係を示す．右辺第2項の総和部分を無視すると次式のようになる．

$$F = v\sqrt{k_n m} \quad (5)$$

式(5)は，式(1)において付加質量の効果を無視（m_c=0）し，等価軸剛性をk_nとした場合に相当する．以下では，式(1)及び式(4)を用いて衝突力を推定し，衝突実験結果と比較する．ただし，本実験では被衝突体の軸剛性は衝突体の軸剛性に比べて十分大きいとし，式(2)右辺第1項は無視した．また，c_lは衝突体の寸法や形状などの衝突体諸元や，衝突力の作用時間やその関数形にも依存する[8]．例えば，Haehnel and Daly[9]は，木材に対し0.22～3.5としており，船舶に対しては0.4がよく用いられている[例えば9]．付加質量は，衝突体周辺の流体運動の影響を質量に置きかえて表すものであり，衝突体の物性値，つまり軸剛性に影響を与えるものではない．すなわち，m_fやc_lの値が，軸剛性に関する以下の議論に影響を与えないと考えられるため，ここではm_c=0として議論を進める．

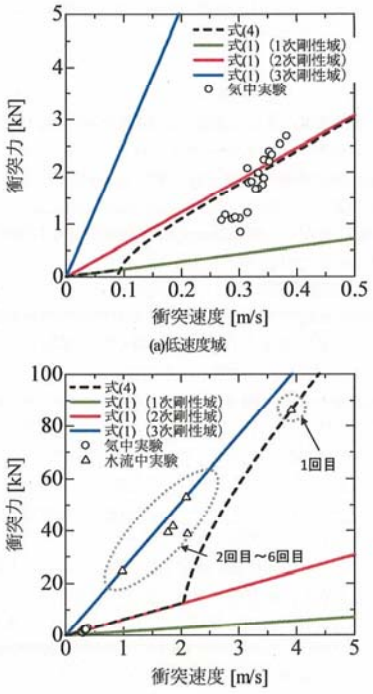

図-9 実験結果と式(4)及び式(1)との比較

図-9に実験で用いた軽自動車に対する式(4)及び式(1)の関係を示す．これらの関係を各剛性域について示し，衝突実験結果も併記した．実験結果と式(4)を比較すると，気中実験では良く一致している．一方，水流中実験では，1回目は良く一致し，2回目以降は過小評価となる．これは，前述のように，3次軸剛性は1回目の計測値に基づいて算出していること，また1回目で1次及び2次剛性域における抵抗力が低下・喪失しており，2回目以降は衝突直後から3次剛性域において荷重に抵抗しているためと考えられる．次に実験結果と式(1)を比較する．2次剛性

域となる低速度域の衝突であった気中実験では，2次軸剛性に基づく式(1)と良い一致を示す．一方，3次剛性域となる高速度域の衝突であった水流中実験では，3次軸剛性に基づく式(1)と2回目以降では良く一致し，1回目においてもやや過大評価となるが，概ね一致している．すなわち，衝突速度に応じて軸剛性が変化する衝突体に対して，衝突速度に応じた軸剛性を選択することにより，式(1)により簡易的かつ合理的に衝突力を評価できる．

(3) 推定手法の適用性検討

式(1)の適用性を検討するため，式(4)の推定結果を真値と仮定し，式(4)と式(1)の差，すなわち，式(4) 右辺第2項の総和部分に着目する．まず，自動車の構造を勘案すると，本研究で用いた軽自動車のように，各剛性域で軸剛性が急増するものと考えられ，$1/k_{n+1}$は$1/k_i$に比べて十分小さく，式(4)は次式のようになる．

$$F = v\sqrt{k_n m}\sqrt{1-\frac{1}{mv^2}\left(\sum_{i=1}^{n-1}\frac{F_i^2}{k_i}\right)} \qquad (6)$$

式(6) 右辺第2項の総和部分は，各次剛性域の軸剛性と最大荷重から計算されるエネルギーの総和と衝突体の運動エネルギーとの比を示している．津波漂流物における衝突速度を勘案すると，本実験結果のように，自動車衝突時には，バンパーやビームの抵抗力は喪失し，それに伴う吸収エネルギーは運動エネルギーに比べて十分小さいことが予想される．つまり，総和部分は0に近づくため，式(6)または式(4)における推定値は，式(1)における推定値に近づく．例えば，水流中実験1回目では，バンパーやビームにおける吸収エネルギーは1324Jに対し，運動エネルギーは5120Jとなり，式(1)による推定値は，式(6)による推定値の$(1-1324/5120)^{1/2}\fallingdotseq 0.86$倍程度となる．式(1)では16%程度過大評価になるものの，簡易的かつ合理的な衝突力評価が可能であると考えられる． ただし，**図-9**からもわかるように，軸剛性域の遷移直後においては，過大評価になることに留意する必要がある．

4. 既往研究における自動車・船舶の軸剛性

(1) 自動車における軸剛性

自動車の安全性評価の指標の一つに，衝突時の乗員を保護する車の能力（衝突安全性）がある．衝突安全性の評価においては，実物の自動車を用いた衝突実験が実施され，衝突時の発生加速度や変形状態，荷重-変位関係等が取得される．ただし，これらの実験における衝突速度は55km/h（≒15.3m/s）であり，津波漂流物における衝突速度に比べて速い．また，鋼材の荷重-変位関係は速度に依存し，高速度ほど軸剛性が高くなる傾向にあるため，以下で示す軸剛性は，津波漂流物における衝突力推定においては安全側評価になることに留意する必要がある．**図-10**に，文献10)，11)とthe National Crash Analysis Center(NCAC)[12]で公開されている荷重-変位関係及び荷重-吸収エネルギー関係に基いて算出した，1次及び2次の軸剛性と各軸剛性域における最大衝突速度の関係を車種ごとに示す．ただし，公開データから読取れるデータは軸剛性，荷重，変形量であるため，変形量と衝突速度の関係式[10]を用いて速度へ換算した．さらに，**表-4**には，調査対象とした車種における，各剛性域の軸剛性及び最大衝突速度の範囲を示した．1次剛性域における最大衝突速度は3.8m/s～9.0m/sであり，多くの津波漂流物が3.0m/s以下で衝突する[13]ことを勘案すると，調査対象とした車種における衝突力は，1次軸剛性により推定できると考えられる．その軸剛性は350～3500kN/mであり，2次軸剛性に比べるとばらつきが小さい．尚，本研究で用いた軽自動車では，メンバーで抵抗する3次軸剛性が**表-4**に示す1次剛性域の軸剛性と同等の値となっている．

表-4 自動車の軸剛性と最大衝突速度の範囲

剛性域	軸剛性[kN/m]	最大衝突速度[m/s]
1次	350～3500	3.8～9.0
2次	1400～12000	5.1～14.8

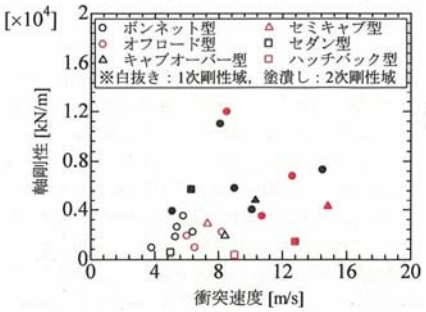

図-10 各次剛性域における最大速度と軸剛性の関係

(2) 船舶における軸剛性

船舶の衝突における安全性に関しては，主に衝突船及び被衝突船のエネルギー吸収性能に関する評価が行われており，実船や模型を用いた衝突実験や有限要素法を用いた数値的検討が行われている．ここでは，文献9)に基づき，比較的小型の総トン数400～4000tonfの船舶（中距離フェリーや小型旅客船，小型貨物船などに相当）における船首衝突時の軸剛性を示す．文献9)では，船首衝突時の破壊形式を模擬した模型実験により荷重-変位関係を取得しており，船首衝突時の荷重-変位関係は，衝突荷重が破壊荷重（圧縮破壊）に達するまでは，一定の割合（軸剛性）で荷重が増加し，その後は一定値（圧縮破壊荷重）を示すとしている．**表-5**に船首の1次軸剛性，

圧縮破壊強度及び圧縮強度に達する衝突速度の例を示す．津波漂流物における速度域においても大きな衝突荷重となり，破壊荷重を超える可能性があることがわかる．

5. まとめ

本論文では，実際の軽自動車を用いた静的載荷実験及び衝突実験を実施し，構造形式や破壊過程に基づいた軸剛性を取得した．この軸剛性は作用する衝突荷重，すなわち，衝突速度に応じて変化する．速度範囲の異なる衝突実験結果から，速度範囲に対応する軸剛性を用いると，既往推定式により簡易的かつ合理的に衝突力が推定可能であることを確認した．なお，衝突時の応答は，衝突位置や向き等の僅かな違いに影響されるため，同条件の衝突実験においても衝突力はばらつく．ただし，このばらつきの範囲は，軸剛性の違いによって生じる衝突力の変化に比べて小さい（**図-9**）．そのため，構造形式等によって決まる軸剛性の範囲を把握することが，衝突力を合理的に推定する上で重要である．

今後は，本論文で示した衝突力推定方法の適用範囲を明確にするとともに，数値実験等により軸剛性のばらつき範囲を検証する．併せて，付加質量係数の実用的な設定方法についても検討する．

謝辞：本実験の実施にあたり，株式会社セレスの富永康彦氏，田山英樹氏，竹内康生氏に多大なるご協力を頂いた．ここに謝意を表する．

表-5 船舶の軸剛性例

船種等	1次軸剛性 [kN/m]	圧縮破壊強度[kN]	衝突速度 [m/s]
総トン数400G.T.船※	5.1×10^3	5.7×10^3	2.30
総トン数1000G.T.船※	6.4×10^3	9.1×10^3	2.30
総トン数2000G.T.船※	8.2×10^3	1.4×10^4	2.31
総トン数4000G.T.船※	1.1×10^4	2.4×10^4	2.34

※文献9)に基づくデータ

参考文献

1) 松冨英夫: 流木衝突力の実用的な評価式と変形特性, 土木学会論文集, No.621/II-47, pp.111-127, 1999.
2) 有川太郎, 織田朋哉, 黒田豊和, 下迫健一郎: 消波工によるケーソン壁面衝突力に関する大規模実験, 海岸工学論文集, 第 50 巻, pp.716-720, 2003.
3) FEMA: Guideline for design of structures for vertical evacuation from tsunami 2nd Edition,FEMA P646, Federal Emergency Management Agency, Washington, D.C., 174p, 2012
4) Haehnel, R.B. and Daly, S.F.: Maximum impact force of woody debris on floodplain structures, *Jounal of Hydraulic Engineering*, ASCE, Vol.130, No.2, pp.112-120, 2004
5) 高畠大輔, 木原直人, 甲斐田秀樹, 宮川義範, 柴山淳, 池野正明: 大規模水理実験による津波フラジリティ評価手法の高度化 (その 2), 電力中央研究所研究報告書, (準備中)
6) 太田一行, 木原直人, 佐藤隆宏, 高畠大輔, 松山昌史, 吉井匠: 任意の流速・浸水深を有する津波氾濫流の再現実験手法, 土木学会論文集 B2(海岸工学), Vol. 69, No.2, pp.1471-1475, 2013.
7) 水野幸次: 自動車の衝突安全, 名古屋大学出版会, 99p., 2012
8) 元良誠三, 藤野正隆, 杉浦正憲, 杉田松次: 衝突時の等価附加質量について, 日本造船学会論文集, 第 126 号, pp.141-152, 1969
9) 有田喜久雄: 船舶等の衝突強度に関する研究, 船舶技術研究所報告, 第 25 巻, 第 1 号, pp.35-125, 1988
10) 久保田正美, 國分善晴: 前面形状別の車体エネルギ吸収特性, 自動車研究, 17-1, pp.19-22, 1995
11) 大賀涼, 井出芳和, 碇孝浩: 自動車アセスメントの試験データを用いた変形エネルギー吸収分布図の作製, 自動車技術会学術講演会前刷集, No.49-07, pp.5-10, 2007
12) The National Crash Analysis Center, http://www.ncac.gwu.edu/about.html
13) 木原直人, 松山昌史, 藤井直樹: 漂流物挙動解析による津波漂流物衝突に関する確率論的評価手法, 土木学会論文集 B2(海岸工学), Vol. 69, No.2, pp.341-345, 2013.

(2015.3.18 受付)

AXIAL STIFFNESS MODEL FOR ESTIMATING FLOATING DEBRIS IMPACT FORCES DUE TO TSUNAMI

Daisuke TAKABATAKE, Naoto KIHARA, Yoshinori MIYAGAWA, Hideki KAIDA, Atsushi SHIBAYAMA and Masaaki IKENO

In this paper, simplified and reasonable estimating method for the floating debris impact force using existing formula is proposed. Although the impact force is estimated using mass of debris, collision velocity and the axial stiffness of debris in existing formula, the axial stiffness is difficult to determine because the axial stiffness varies depending on collision velocity. To investigate the way how to determine the axial stiffness of debris such as cars, the static loading test and collision test are carried out using actual mini car. Although the axial stiffness of mini car obtained by experiments varies depending on collision velocity, the estimated impact force using exiting formula with axial stiffness to the corresponding collision velocity agrees with experimental results.

３．コメント回答③（FEMA の算定式における係数 1.3 の扱いについて，再検討すること。）

FEMA（2012）における係数 1.3 は，ASCE（American Society of Civil Engineers）による設備の重要度に応じた安全係数であり，重要施設として指定されているビル・構造物に対する係数となっている。

東海第二発電所における津波防護施設の設計においては,係数 1.3 を考慮し,FEMA(2012)により車両の漂流物荷重を算定する。

漂流物荷重算定時に用いる付加質量係数 C は，FEMA（2012）においては図－2 に示す通りとなっており，車両の付加質量係数 C は記載がない。

高畠ら（2015）※2では，水流中衝突実験では，衝突荷重を測定し，その荷重を$F = v\sqrt{km}$で再現するように車両の質量 m を一定とした上で，軸剛性 k を求めている。ここでは，３段階の軸剛性のうち，最も軸剛性が大きい３次剛性 k_3（2.04×10^6 N/m）を用いるものとする。

Table 6-1 Mass and Stiffness of Some Waterborne Floating Debris

Type of Debris	*Mass (m_d) in kg*	*Hydrodynamic Mass Coefft. (c)*	*Debris Stiffness (k_d) in N/m*
Lumber or Wood Log – oriented longitudinally	450	0	2.4 x 10^6 *
20-ft Standard Shipping Container – oriented longitudinally	2200 (empty)	0.30	85 x10^6 **
20-ft Standard Shipping Container – oriented transverse to flow	2200 (empty)	1.00	80 x10^6 **
20-ft Heavy Shipping Container – oriented longitudinally	2400 (empty)	0.30	93 x10^6 **
20-ft Heavy Shipping Container – oriented transverse to flow	2400 (empty)	1.00	87 x10^6 **
40-ft Standard Shipping Container – oriented longitudinally	3800 (empty)	0.20	60 x10^6
40-ft Standard Shipping Container – oriented transverse to flow	3800 (empty)	1.00	40 x10^6

* Haehnal and Daly, 2002; ** Peterson and Naito, 2012

図－2　FEMA（2012）における流木及びコンテナの付加質量

表－3 に船舶，流木及び車両の漂流物荷重一覧を示す。

漂流物荷重の算定に用いる流速は，基準津波時 11　m/s，T.P.+24m 津波時は 15　m/s とした。

船舶は道路橋示方書式により漂流物荷重を算定した。

流木の漂流物荷重は，松冨ほか，有川ほかの式による算定に加え，FEMA（2012）の式$F_i = 1.3u_{max}\sqrt{km_d(1+c)}$により係数 1.3 を考慮し，図－2 に示す FEMA（2012）に記載されている流木の軸剛性 2.4×10^6 N/m を用いた。

車両の漂流物荷重は，係数 1.3 及び設計上の保守的な配慮として図－2 に示される FEMA（2012）において最大の付加質量係数 C= 1.0 を用いて，FEMA 式における最大の荷重を算定した。

算出の結果，漂流物荷重は，基準津波時（流速 11m/s）では 759kN，T.P.+24m 津波時（流速 15m/s）では 1035kN となり，これらを設計用漂流物荷重とする。

表－3　漂流物荷重一覧

種類	質量 (t)	適用式	漂流物荷重（kN）	
			基準津波時 (流速11 m/s)	T.P.+24 m津波時 (流速15 m/s)
船舶	15	道路橋示方書	162	221
流木	0.08	松冨ほか	157	226
		FEMA	198	270
		有川ほか	390	565
車両	0.69	FEMA (C=1.0)	759	1035

※1：大規模水理実験による津波フラジリティ評価手法の高度化（その２）－津波漂流物の衝突力評価手法の適用性検証－研究報告ｏ15003，電力中央研究所報告書（2015）

※2：高畠ら：津波漂流物の衝突力推定における軸剛性モデル，土木学会論文集 B2（海岸工学）（2015）

※3：Haehnel R.R and Daly F.D.：Maximum Impact Force of Woody Debris on Floodplain Structures.Journal of Hydraulic Engineering，130，No.2，2004，pp.112-120.

以上